**Article**

# Fermi edge singularity in neutral electron–hole system

In the format provided by the
authors and unedited

D. J. Choksy*,[1] E. A. Szwed*,[1] L. V. Butov,[1] K. W. Baldwin,[2] and L. N. Pfeiffer[2]

[1]*Department of Physics, University of California at San Diego, La Jolla, CA 92093, USA*
[2]*Princeton University, Princeton, New Jersey 08544, USA*
(Dated: April 27, 2023)

PACS numbers:

## Supplementary Note 1: CQW heterostructure

The CQW heterostructure (Fig. 1b) is grown by molecular beam epitaxy. CQW consists of two 15-nm GaAs QWs separated by a 4-nm $Al_{0.33}Ga_{0.67}As$ barrier. $n^+$ GaAs layer with $n_{Si} \sim 10^{18}$ cm$^{-3}$ serves as a bottom electrode. The CQW is positioned 100 nm above the $n^+$ GaAs layer within the undoped 1-$\mu$m-thick $Al_{0.33}Ga_{0.67}As$ layer. The CQW is positioned closer to the homogeneous bottom electrode to suppress the fringing in-plane electric field in excitonic devices [1]. The top semitransparent electrode is fabricated by applying 2-nm Ti and 7-nm Pt on a 7.5-nm GaAs cap layer. Applied gate voltage $V_g = -2.5$ V creates an electric field in the $z$ direction.
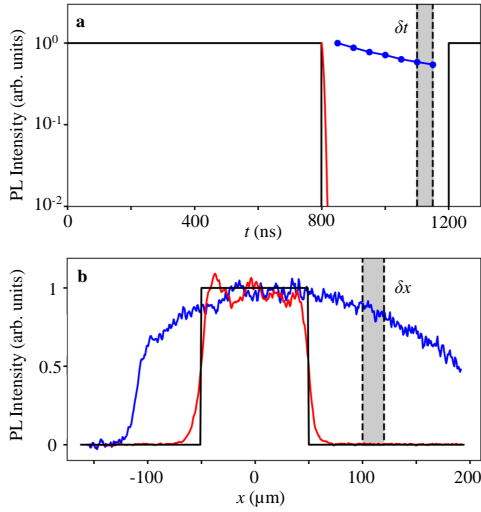


FIG. S1: Optical measurements. (a) The e-h system is generated by laser pulses 800 ns on, 400 ns off (shown schematically by black line). The measurements are performed $\delta t = 300$ ns after the laser excitation pulse within $\tau_w = 50$ ns window (gray area). (b) The laser excitation spot is mesa-shaped (shown schematically by black line). The measurements are performed $\sim 50$ $\mu$m away from the edge of the mesa-shaped laser excitation spot within $\sim 20$ $\mu$m window (gray area). $x \sim -100$ $\mu$m corresponds to the device edge. The DX PL (red line) closely follows the laser excitation in time (a) and space (b) due to the short DX lifetime. The I-EHP PL (blue line and dots) extends in time (a) and space (b) due to the long I-EHP lifetime.
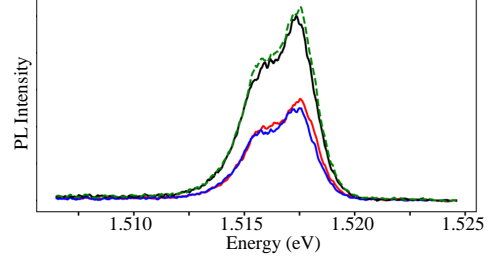


FIG. S2: Variation of the spectra within the signal accumulation window. The I-EHP spectrum measured during the 50 ns window (black line) and during the first half (red line) and within the second half (blue line) of the window. The sum of the spectra within the half-windows (green dashed line) is close to the spectrum within the window (black line). These measurements show that the spectrum variation during the window is negligibly small.

## Supplementary Note 2: Optical measurements

The experiments are designed to facilitate lowering the temperature of the optically generated e-h system, as outlined in the main text. The creation of cold I-EHP is facilitated by separating the e-h plasma from the laser excitation in space and time: (i) The measurements are performed $\delta t = 300$ ns after the laser excitation pulse within $\tau_w = 50$ ns window (Fig. S1a). This delay $\delta t$ allows for cooling the photoexcited e-h system to low temperatures close to the lattice temperature. At the same time, $\delta t \sim \tau$ and $\tau_w << \tau$ enable the density staying high and nearly constant during the measurements. (ii) The measurements are performed $\sim 50$ $\mu$m away from the edge of the mesa-shaped laser excitation spot (Fig. S1b). This separation further facilitates cooling of the photoexcited e-h system. At the same time, the density in the signal detection region does not drop substantially in comparison to the excitation region since the separation is shorter than the I-EHP (and IX) propagation length in the heterostructure (Fig. S1b). To further reduce the heating of e-h system, the laser excitation is resonant to the direct exciton energy ($E_{ex} \sim 1.545$ eV). The resonant excitation increases absorption for a fixed $P_{ex}$ and minimizes the energy of photoexcited e-h pairs. The laser
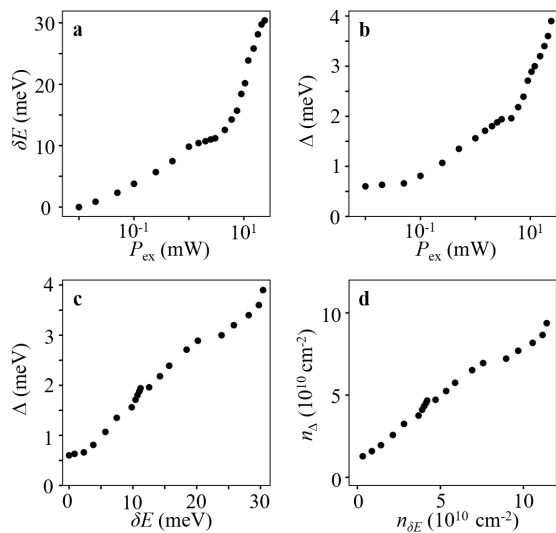
FIG. S3: PL energy shift and linewidth. (a) The PL energy shift $\delta E$ vs. $P_{\text{ex}}$. $\delta E$ is counted from the IX energy at the lowest $P_{\text{ex}}$. (b) The PL linewidth $\Delta$ (full-width-half-maximum) vs. $P_{\text{ex}}$. (c) $\Delta$ vs. $\delta E$. (d) $n$ estimated from $\Delta$ vs. $n$ estimated from $\delta E$. $T = 2$ K for all data. The estimates use $\delta E = 4\pi e^2 dn/\varepsilon$ and $\Delta \sim E_{\text{Fe}} + E_{\text{Fh}} = \pi\hbar^2 n(1/m_{\text{e}} + 1/m_{\text{h}})$. The estimates from $\delta E$ and from $\Delta$ give similar $n$.

pulses are 800 ns on, 400 ns off. The off time is longer than $\delta t$ to enable the cooling, yet is as short as possible, just longer than $\delta t + \tau_{\text{w}}$, to enhance the density for a given $P_{\text{ex}}$.

The e-h system is generated by a Ti:Sapphire laser ($E_{\text{ex}} \sim 1.545$ eV). An AOM is used for making laser pulses 800 ns on, 400 ns off (Fig. S1a). The mesa-shaped laser excitation spot with $\sim 100$ $\mu$m diameter is formed using an axicon (Fig. S1b). The DX PL closely follows the laser excitation in time (Fig. S1a) and space (Fig. S1b) due to the short DX lifetime. The I-EHP (and IX) PL extends in time (Fig. S1a) and space (Fig. S1b) due to the long I-EHP (and IX) lifetime.

The 50 ns window is long enough to collect sufficient I-EHP (or IX) signal yet much shorter than the I-EHP (or IX) lifetime so the signal variation during the window is negligibly small. To verify this, the measurements were performed within the first half and within the second half of the window and these measurements show similar spectra (Fig. S2).

The PL spectra are measured using a spectrometer with resolution 0.2 meV and a liquid-nitrogen-cooled CCD coupled to a PicoStar HR TauTec time-gated intensifier. The experiments are performed in a variable-temperature 4He cryostat.
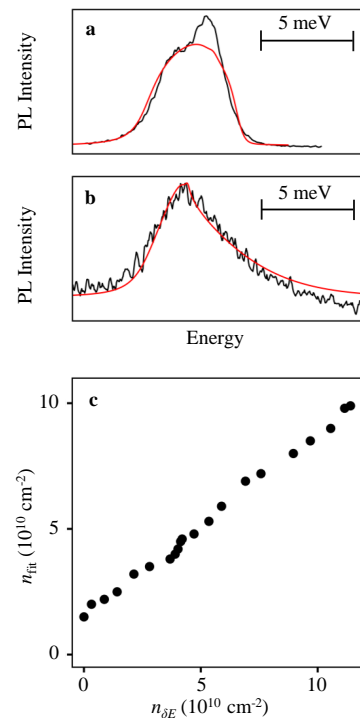


FIG. S4: Simulations of I-EHP PL spectra. (a,b) The simulated I-EHP PL spectra without taking into account the Fermi edge singularity (red lines) and the measured I-EHP PL spectra (black lines). $T = 2$ K and $P_{\text{ex}} = 24$ mW, $T_{\text{fit}} = 2$ K and $n_{\text{fit}} = 10^{11}$ cm$^{-2}$ (a). $T = 25$ K and $P_{\text{ex}} = 24$ mW, $T_{\text{fit}} = 25$ K and $n_{\text{fit}} = 7.6 \times 10^{10}$ cm$^{-2}$ (b). (c) $n$ estimated from the PL spectrum fit vs. $n$ estimated from $\delta E$, $T = 2$ K.

**Supplementary Note 3: PL energy shift and lineshape**

The density $n$ in I-EHP can be estimated from the PL energy shift $\delta E$ using the "capacitor" formula $\delta E = 4\pi e^2 dn/\varepsilon$. $n$ in I-EHP can be also estimated from the PL linewidth $\Delta \sim E_{\text{Fe}} + E_{\text{Fh}} = \pi\hbar^2 n(1/m_e + 1/m_h)$. The estimates from $\delta E$ and from $\Delta$ give similar $n$ in the high-density regime, $n \gtrsim 4 \times 10^{10}$ cm$^{-2}$ (Fig. S3d). The estimates extended to the low-density regime show a deviation from this similarity, increasing for lower densities (Fig. S3d). The deviation is expected since in the low-density regime, the equation for $\delta E$ is less accurate and $\Delta$ is determined by the homogeneous and inhomogeneous IX broadening, as outlined in the main text.

The I-EHP PL spectra are simulated without taking into account the Fermi edge singularity and compared with the measured I-EHP PL spectra (Fig. S4). The simulations are outlined below. Due to the small photon momentum, the optical transition occur for the same absolute values of electron and hole momenta $k_{\text{e}} = k_{\text{h}}$. For the constant 2D density of states, the PL intensity at energy $E_i = \frac{\hbar^2 k_i^2}{2m_{\text{e}}} + \frac{\hbar^2 k_i^2}{2m_{\text{h}}}$ is determined by the product of the electron and hole distribution functions $I(E_i) \propto$
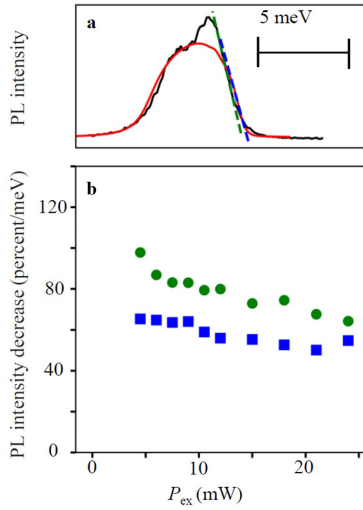
FIG. S5: Comparison of the sharpness of the high-energy side of the spectrum in the simulations and in the experiment in the high-density I-EHP regime. (a) The simulated I-EHP PL spectrum without taking into account the Fermi edge singularity (red line) and the measured I-EHP PL spectrum (black line). The dashed green (blue) line shows the sharpest PL intensity decrease on the high-energy side of the spectrum in the experiment (simulation). $T = 2$ K and $P_{ex} = 24$ mW, $T_{fit} = 2$ K and $n_{fit} = 10^{11}$ cm$^{-2}$. (b) The sharpest PL intensity decrease on the high-energy side of the spectrum in the experiment (green circles) and in the simulation (blue squares). The sharpness is similar indicating that the temperature of the dense optically created e-h system lowers to the bath temperature in the experiments $T_{eh} \sim 2$ K.

$f_e(k_i)f_h(k_i)$, where $E_i$ is counted from the lowest PL energy, $k_i = k_e = k_h$, $f_{e,h} = \left(\exp \frac{\hbar^2(k_i^2 - k_F^2)}{2m_{e,h}k_B T} + 1\right)^{-1}$, $k_F$ the Fermi momentum. For low temperatures $k_B T \ll E_{Fe}, E_{Fh}$, the PL line $I(E_i)$ is step-like with the sharp steps both on the low-energy side and the high-energy side and the width $\Delta \sim E_{Fe} + E_{Fh} = E_F$. The step sharpness on the high-energy side is determined by the temperature. To account for the finite step sharpness on the low-energy side the following approximation is used. $I(E_i)$ is convolved with $\frac{\gamma(E_i)}{\pi} \frac{1}{(E - E_i)^2 - \gamma(E_i)^2}$ describing the damping of one-particle states [2], where the broadening parameter $\gamma(E_i)$ is assumed to decrease to zero at the Fermi level as $(E_F - E_i)^2$ [3].

At high temperatures, the simulated and measured I-EHP spectra are close, with the intensity reduction at the high-energy side following the thermal distribution (Fig. S4b). At low temperatures, the simulations show step-like I-EHP spectra with the linewidth $\Delta \sim E_{Fe} + E_{Fh}$, similar to the spectra of spatially direct EHP in single QWs [4], and the measured I-EHP PL is strongly enhanced at the Fermi energy in comparison to the simulations due to the Fermi edge singularity (Fig. S4a).
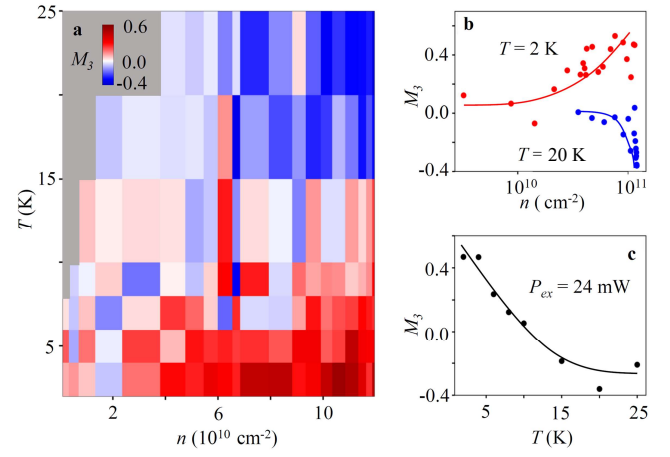


FIG. S6: The spectrum skewness $M_3$. (a) $M_3$ vs. density and temperature. The density $n$ is estimated from the energy shift $\delta E = 4\pi e^2 dn/\varepsilon$. (b) $M_3$ vs. $n$ at $T = 2$ K and 20 K. (c) $M_3$ vs. temperature at $n = 10^{11}$ cm$^{-2}$. The lines are guides to the eye. The Fermi edge singularity characterized by high positive $M_3$ is observed in dense I-EHP at low temperatures.

For the dense I-EHP, the density $n_{fit}$ estimated from the PL spectrum fit is close to the density estimated from the energy shift $\delta E$ (Fig. 4c). $n_{fit}$ (Fig. 4c) is close to the density estimated from the PL linewidth $\Delta$ (Fig. 3d).

The e-h temperature $T_{eh}$ in the high-density I-EHP regime can be estimated from the sharpness of the high-energy side of the spectrum. The simulations were performed for the bath temperature in the experiment and the sharpness of the high-energy side in the simulations and in the experiment are close (Fig. S4a), indicating that the temperature of the dense optically created e-h system lowers to the bath temperature in the experiments $T_{eh} \sim 2$ K. This is further supported by Fig. S5 presenting the sharpness of the high-energy side of the spectrum in the simulations and in the experiment for different densities in the I-EHP regime ($P_{ex} \gtrsim 4$ mW). Figure S5 shows that the sharpness in the simulations and in the experiment are similar, indicating that the temperature of the dense optically created e-h system lowers to the bath temperature in the experiments $T_{eh} \sim 2$ K. A higher sharpness corresponds to a lower temperature and Fig. S5 shows that the sharpness is even higher in the experiment. A higher sharpness in the experiment may be related to neglecting the excitonic effects in the simulations.

**Supplementary Note 4: The spectrum skewness $M_3$**

Figure S6 shows the spectrum skewness $M_3$ vs. temperature and density. This figure is similar to Fig. 3 showing $M_3$ vs. temperature and $P_{ex}$. The density $n$ is estimated from the energy shift $\delta E = 4\pi e^2 dn/\varepsilon$. Figure S6
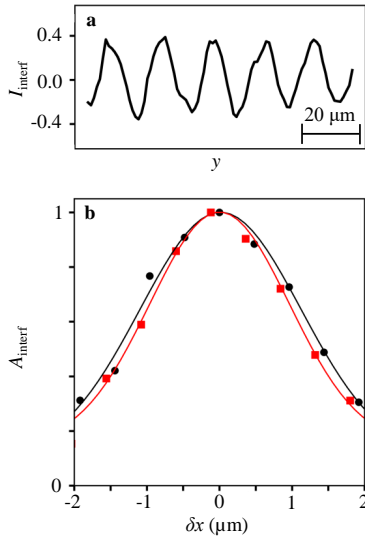
FIG. S7: Shift-interferometry measurements. (a) Interference fringes $I_{interf}(y)$ for $\delta x = 1.5$ $\mu$m, $T = 2$ K, $P_{ex} = 2.5$ mW. (b) The amplitude of interference fringes $A_{interf}$ vs. $\delta x$ for $P_{ex} = 2.5$ mW (black points) and 0.2 mW (red squares), $T = 2$ K. Gaussian fits are shown by the black and red lines, respectively.

shows that the Fermi edge singularity characterized by high positive $M_3$ is observed in the dense I-EHP at low temperatures, that is in the high-$n$ – low-$T$ part of the $n - T$ diagram.

**Supplementary Note 5: Shift-interferometry measurements**

In the shift-interferometry measurements, a Mach-Zehnder interferometer is added in the signal detection path as in Ref. [5]. The spectrometer grating is replaced by a mirror and an interference filter of linewidth 5 nm adjusted to the I-EHP (or IX) PL wavelength is added to select the entire I-EHP (or IX) PL line for the studied $P_{ex}$ and $T$. The rest of the laser excitation and signal detection, outlined above, is kept unchanged.

The emission images produced by each of the two arms of the Mach-Zehnder interferometer are shifted relative to each other along $x$ to measure the interference between the emission of I-EHPs (or IXs), which are separated by $\delta x$ in the layer plane. $I_{interf} = (I_{12} - I_1 - I_2)/(2\sqrt{I_1 I_2})$ is calculated from the measured PL intensity $I_1$ for arm 1 open, $I_2$ for arm 2 open, and $I_{12}$ for both arms open (Fig. S7a). In "the ideal experiment", the amplitude of interference fringes $A_{interf}(\delta x)$ gives the first order coherence function $g_1(\delta x)$ and the width of $g_1(\delta x)$, the coherence length, quantifies spontaneous coherence in the system [5]. In practice, the measured $A_{interf}(\delta x)$ is given by the convolution of $g_1(\delta x)$ with the point-spread function (PSF) of the optical system in the experiment [6]. The CQW contain no point source for the precise measurement of PSF. NA = 0.27 of the objective in the experiment gives a lower estimate for PSF width $\xi_{PSF} \sim 0.9$ $\mu$m for the optical system. The dependence of $\xi$ on the parameters shows that the coherence length in the e-h system is sufficiently large in comparison to the spatial resolution of the optical system $\xi_{PSF}$. Otherwise, the measured $\xi$ would be determined by $\xi_{PSF}$ and practically would not depend on the parameters [6]. Figure 7b shows examples of the measured $A_{interf}(\delta x)$. $\xi$ are taken as the half-widths at $1/e$ height of Gaussian fits to $A_{interf}(\delta x)$.

*equal contribution

**References**

[1] A.T. Hammack, N.A. Gippius, Sen Yang, G.O. Andreev, L.V. Butov, M. Hanson, A.C. Gossard, Excitons in electrostatic traps, *J. Appl. Phys.* **99**, 066104 (2006).

[2] P.T. Landsberg, Electron Interaction Effects on Recombination Spectra, *Phys. Stat. Sol.* **15**, 623 (1966).

[3] Sankar Das Sarma, Yunxiang Liao, Know the enemy: 2D Fermi liquids, *Annals of Physics* **435**, 168495 (2021).

[4] L.V. Butov, V.D. Kulakovskii, E. Lach, A. Forchel, D. Grützmacher, Magnetoluminescence study of many-body effects in homogeneous quasi-two-dimensional electron-hole plasma in undoped InGaAs/InP single quantum wells, *Phys. Rev. B* **44**, 10680 (1991).

[5] A.A. High, J.R. Leonard, A.T. Hammack, M.M. Fogler, L.V. Butov, A.V. Kavokin, K.L. Campman, A.C. Gossard, Spontaneous coherence in a cold exciton gas, *Nature* **483**, 584 (2012).

[6] M.M. Fogler, Sen Yang, A.T. Hammack, L.V. Butov, A.C. Gossard, Effect of spatial resolution on the estimates of the coherence length of excitons in quantum wells, *Phys. Rev. B* **78**, 035411 (2008).